Publ. Astron. Soc. Japan 25, 207-229 (1973)

Radio Spurs and Spiral Structure of the Galaxy. I. Optical and Radio Brightness Distributions in the Milky Way

Yoshiaki SOFUE

Department of Physics, Nagoya University, Chikusa, Nagoya

(Received 1972 August 28; revised 1972 October 19)

Abstract

A clear correlation is found between the positions of galactic radio spurs, optically obscured regions (dark patches) in the Milky Way, and tangential directions of the spiral arms. This correlation suggests that the spurs are physically connected with dense interstellar gas along the spiral arms of the Galaxy.

The galactic radio spur is interpreted as a nonthermal emission from a halo of magnetic fields and relativistic electrons, distributed above galactic shock wave region. The spur is produced by inflation of magnetic fields with relativistic electrons out of the spiral arm in which the inflation is triggered by the galactic shock wave. The optically dark regions are considered to result from tangential viewing of the galactic shock wave at the spiral arm, where the interstellar gas including the dust grains is strongly compressed.

Key words: Galactic shock waves; Milky Way; Radio spurs; Spiral arms.

1. *Introduction*

If we look at the Milky Way, it is easy to find a dark lane along the galactic equator as well as darker patches superimposed on it. A dark area at $l=20°$ to $30°$ and $b \gtrsim 0°$ is remarkable (figure 1). It should be noticed that the well-known North Polar Spur at radio continuum seems to extend up to higher latitudes from the center of this large dark region. No author seems to have paid systematic attention to the spatial correlations between radio spurs and dark obscurations of diffuse starlight in the Milky Way, although some workers have discussed the spatial correlation of the spurs with neutral hydrogen spurs (BERKHUIJSEN, HASLAM, and SALTER 1970, 1971).

It is the purpose of the present paper to show a clear spatial correlation between the locations of dark obscurations in the Milky Way and of the galactic radio spurs, as well as the neutral hydrogen spurs. It will be demonstrated that the spurs are associated with compressed interstellar gas along the galactic spiral arms (section 2). Sections 3 and 4 are devoted to interpretations of these correlations on the basis of spiral structure and the galactic shock wave theory (FUJIMOTO 1966; ROBERTS 1969; ROBERTS and YUAN 1970; TOSA 1973). In section 3, we propose that the local dark regions in the Milky Way are the result of the tangential viewing of the galactic shock waves in which the absorbing matter as well as the interstellar gas is compressed. Model calculations of the distribution of diffuse starlight confirm this proposal. In section 4, a new model is proposed, in which the nonthermal radio spurs are due to cosmic ray electrons and magnetic

fields projected into the galactic halo out of the galactic arms. The projection or inflation of magnetic bubbles out of the gaseous disk is excited in the galactic shocked region along the spiral arm. Model calculation of the distribution of nonthermal radio emission will reproduce the observed spurs. Section 5 is devoted to discussions of current theories of spurs with particular regards paid to the supernova remnant hypotheses (HANBURY BROWN, DAVIES, and HAZARD 1960; ODA and HASEGAWA 1962).

2. *Spatial Correlation of Dark Regions in the Milky Way, Radio Spurs, and the Spiral Arms*

In this section we will show that there exists a good spatial correlation between locally obscured regions in the Milky Way, galactic spurs, neutral hydrogen spurs, the tangential directions of the galactic arms, and the Mills steps in meter-wavelength radiation.

(i) Spatial correlation between dark regions and radio spurs.

Figure 2a shows isophotes of the radio brightness temperature at a wavelength of 75 cm obtained by SEEGER, STUMPERS, and VAN HURCK (1966). Radio spurs are shown by hatched areas. In addition to the well-known radio spurs such as North Polar Spur, Cetus Arc, and Loop III, there are many recognizable spurs.

A contour diagram of the column densities of the neutral hydrogen gas (MCGEE, MURRAY, and MILTON 1963; TAKAKUBO and VAN WOERDEN 1966; TOLBERT 1971)* is shown in figure 2b. Hatched regions indicate neutral hydrogen spurs. We find that almost of them are located nearly at the same positions as the radio continuum spurs. The spatial correlation of the North Polar Spur at radio continuum with a neutral hydrogen spur at $l \approx 30°$ has already been pointed out by BERKHUIJSEN et al. (1970).

Figure 3 shows the isophotes of the diffuse starlight brightness obtained by visual range photometry (ELSÄSSER and HAUG 1960), where we find many local obscured regions which are recognized as dips of contour lines toward the equator (horizontally-hatched regions). In this figure are also superimposed the locations of radio continuum and neutral hydrogen spurs (see also table 1). A good spatial correlation can be recognized between radio spurs, neutral hydrogen spurs and optically dark regions. (An optically obscured region whose center is located at the galactic coordinates (l, b) will be hereafter referred to as Dark Region (l, b)). Radio continuum spurs and neutral hydrogen spurs will be referred to as Radio- and HI-spurs, respectively.) This spatial correlation suggests that a radio spur is associated with a region of dense interstellar gas.

(ii) Radio spurs and dark regions associated with the spiral arms of the Galaxy.

The galactic longitudes of the tangential directions of the neutral hydrogen arms derived by KERR and WESTERHOUT (1965) are indicated with the thick arrows in figure 3. The directions of MILLS (1959) steps in the distribution of radio continuum emission at 3.5 m wavelength along the galactic equator are also indicated by the thin arrows. It should be noticed that these directions coincide in longitude

* Dr. T. Kato has completed the whole sky map of the column density of neutral hydrogen gas, making use of the values obtained by these authors. The present author thanks her for permitting him to use it before publication.

Table 1. Summary of spatial correlation among optical dark regions, Radio-spurs, HI-spurs, Mills steps, and tangential directions of HI-arms. Each object is indicated by its (l, b) or by the proper name.

Dark region (l, b)	Radio-spur (l, b)	HI-spur (l, b)	Mills step (l)	HI-arm (l)	Comment
Northen hemisphere					
(0+05)....	(0+10)-(355+20)	(12+10)-(352+40)	359		Galactic center
(13+00)....	(15+13)- (03+27)		13		
(25+05)....	(27+10)- (30+50)	(30+20)- (33+50)	27.5	Anti-Orion bridge: 25-30	North Polar Spur (Loop I)
(55+05)....	(45+05)- (50+25)		40-50	Sagittarius arm: 50	
(92+07)....	(87+15)-(105+50)	(80+10)- (80+60)	80: Cygnus maximum	Cygnus arm	Loop III
(153+00)....	(154+10)-(150+50)	(150+25)-(140+40)		Maximum in Perseus arm	Loop III
(265+03)....	(265+15)-(265+45)	(265+15)-(275+25)	262: Vela-Puppis maximum	Cygnus arm	Loop I
(320+05)....			327	Sagittarius arm: 315-330	
(340+05)....	(352+13)-(345+20)	(350+12)-(340+22)	344		
Southern hemisphere					
....	(10−13)- (15−30)	(10−10)- (15−30)	13		
....	(48−10)- (50−25)	(48−10)- (50−30)	40-50	Sagittarius arm: 50	Cetus Arc (Loop II)
....	(45−30)- (40−50)	(30−30)- (50−70)			
(70−05)....	(70−13)- (82−50)	(70−13)- (75−27)	80: Cygnus maximum	Cygnus arm	
....	(152−20)-(130−50)	(157−10)-(158−25)		Maximum in Perseus arm	Cetus Arc (Loop II)
(180−05)....	(185−15)-(170−25)	(187−10)-(180−70)			
(340−05)....		(337−17)-(342−32)	337 or 344		

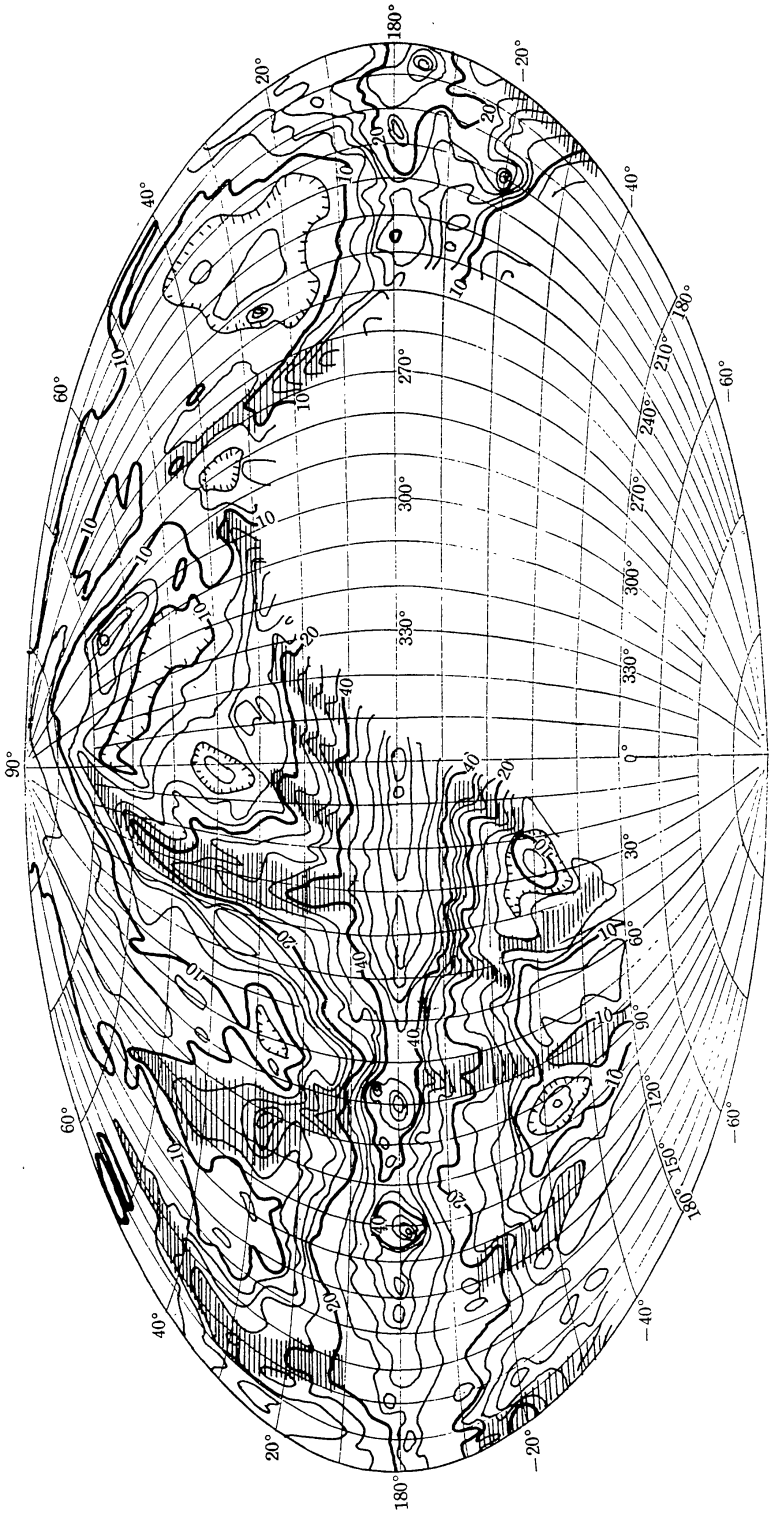

Fig. 2a. Isophotes of the brightness temperature of the sky at $\lambda 75$ cm radio continuum in the (l, b)-plane, reproduced from SEEGER, WESTERHOUT CONWAY, and HOEKEMA (1965). Numerals on the contours are in units of 1.3 K. Hatched areas indicate the radio spurs.

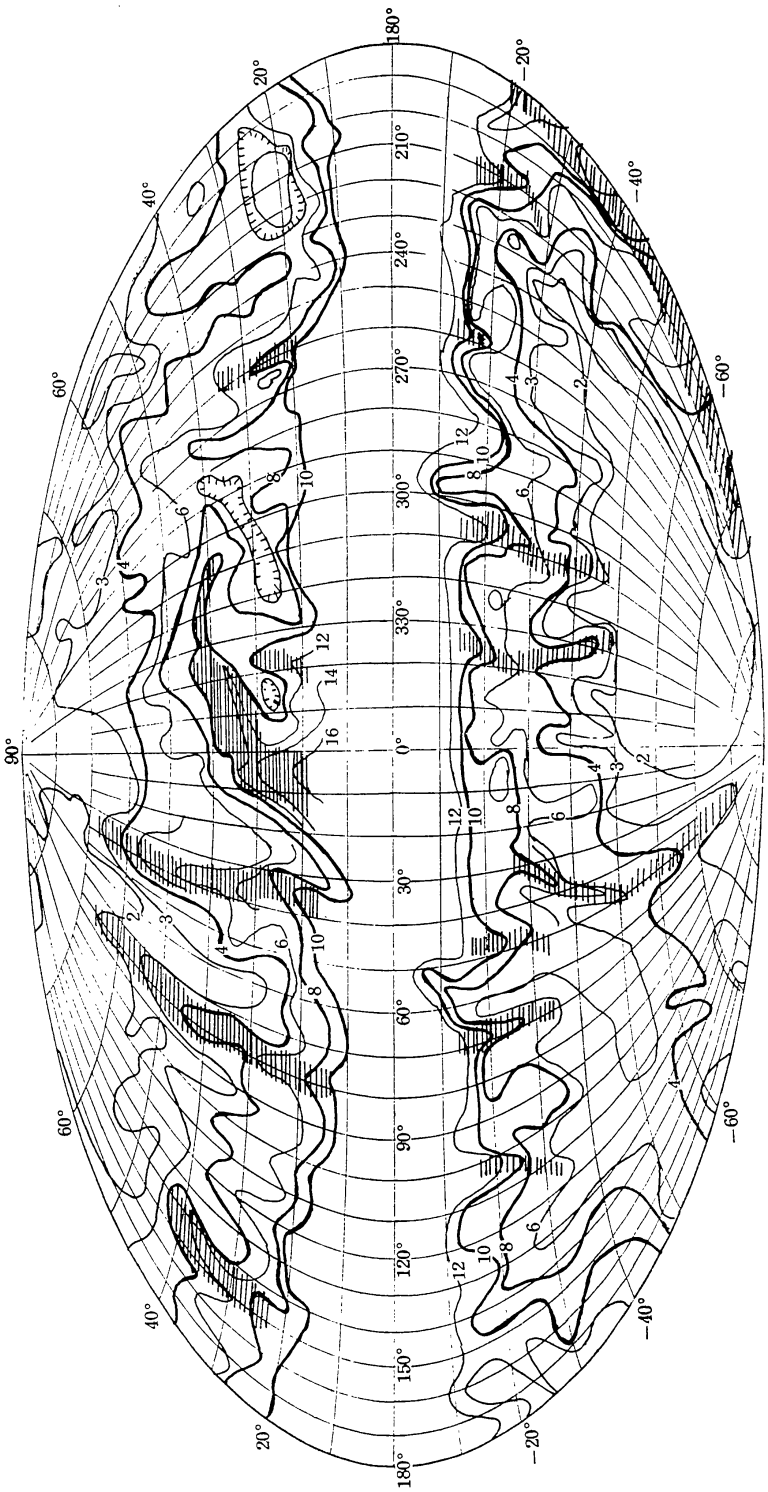

Fig. 2b. Contours of the equal column density of neutral hydrogen gas (McGee, Murray, and Milton 1963; Takakubo and van Woerden 1966; Tolbert 1971; the whole sky map is due to Dr. T. Kato). Numerals on the contours are in units of 10^{20} atoms cm^{-2}. Shaded areas show the H I-spurs.

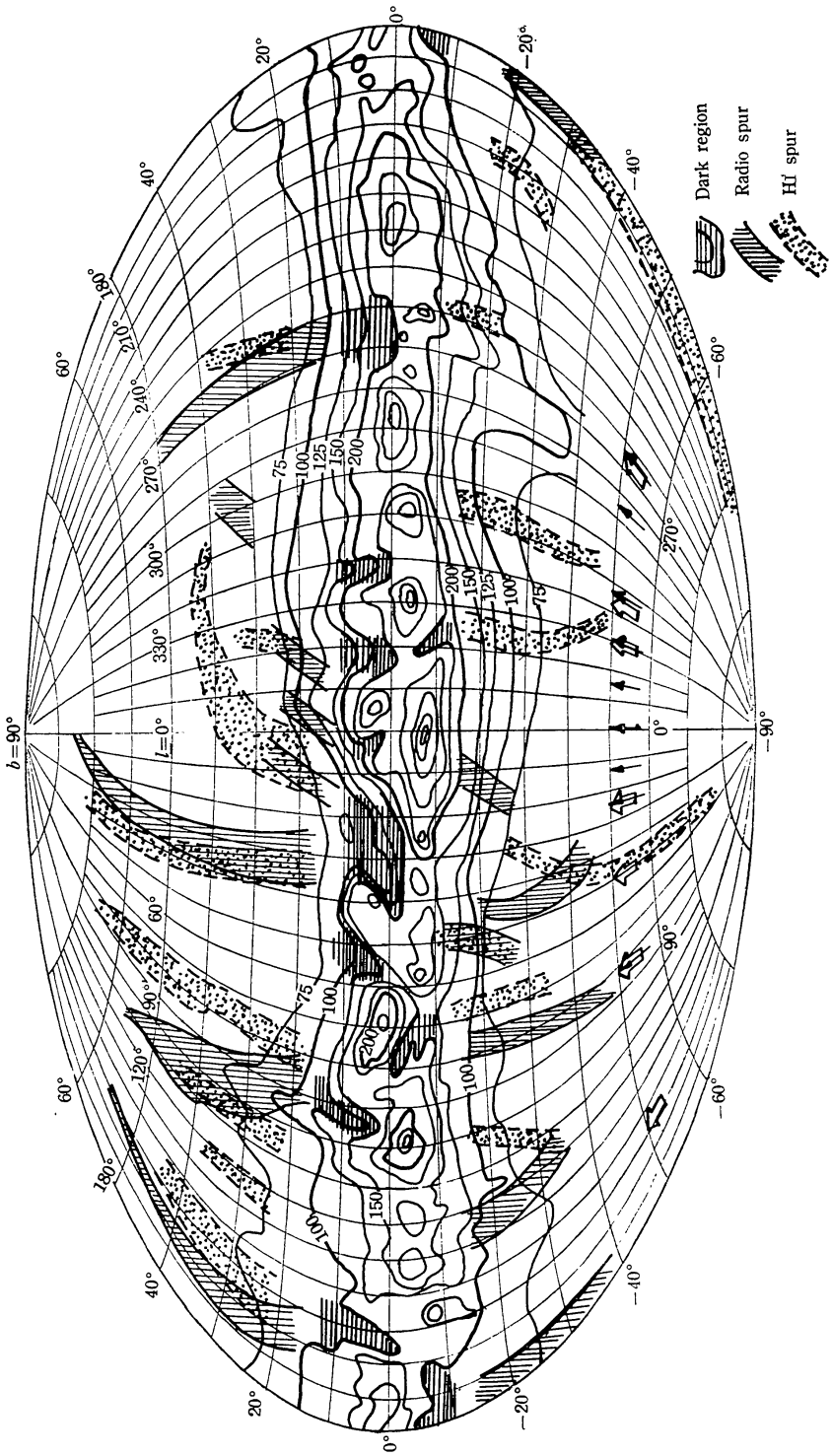

Fig. 3. Isophotes of photo-electric survey of the Milky Way in the visual range, reproduced from ELSÄSSER and HAUG (1960). Indicated numerals on the contours are in units of the number of 10 mag stars/square degree. Optical dark regions are indicated by hatched areas. Positions of radio spurs and HI-spurs are superimposed. Thin arrows indicate the longitudes of the Mills steps, and thick arrows indicate the tangential directions of spiral arms.

with directions of the dark regions and the radio spurs.

The Dark Region (90+10) accompanying Radio- and H I-spurs at (l=90°-100°) and Dark Region (265+03) accompanying Radio-spur at (l=260°-270°) coincide in galactic longitudes with the tangential directions of the Cygnus arm (l=80°) and with its opposite direction (l=260°), respectively. They also coincide, respectively, with the Cygnus maximum (l=80°) and the Vela-Puppis maximum (l=262°) observed at 3.5 m wavelength emission (MILLS 1959). The great Dark Region (25+05) and the North Polar Spur (l=30°) coincide with the anti-Orion bridge of neutral hydrogen gas in the direction of l=25°, which is also directed nearly to Mills step at l=27°.5. Here we have referred to the bridge-like feature extending to l=25° and linking the Cygnus arm and the Sagittarius arm, in the map of the distribution of neutral hydrogen arm in the Galaxy (KERR and WESTERHOUT 1965), as the anti-Orion bridge. These situations of coincidence are, together with other spurs and dark regions, summarized in table 1.

From these facts, we can conclude that the dark regions and the radio spurs are physically related to the spiral structure of the Galaxy. In particular, the correlation of radio spurs with the dark regions suggests that the spurs are situated above regions with compressed interstellar gas along the galactic arms. The spatial coincidence of dark regions with the distant inner arms near the galactic center will, however, be due only to chance coincidence, since it is unrealistic to assume that such distant arms contribute to the starlight absorption in the Milky Way.

3. *Interpretation of the Optical Dark Regions in Connection with the Galactic Shock Wave*

In the present and next sections, we will give a new interpretation of the dark regions and the radio continuum spurs on the basis of the galactic shock wave theory.

The formation of a galactic shock wave (shock lane) in the interstellar gas along the spiral arm has been demonstrated by FUJIMOTO (1966) on the basis of the spiral pattern theory. He has shown that the gas is compressed at the shock front by a factor of 5 to 10 times the mean density, and that the width of the shocked region is about one fifteenth the interval between neighboring spiral arms. ROBERTS (1969) and ROBERTS and YUAN (1970) have developed this study in more realistic way giving essentially the same results as FUJIMOTO (1966). TOSA (1973) has extended the theory to the case in which a vertical spread of the distribution of the gas from the galactic plane is taken into account.

It is reasonable to consider that absorbing matter is correspondingly abundant at the shocked region. If we adopt 0.5 to 1 mag kpc^{-1} as an extinction coefficient for starlight in normal interstellar space, then the extinction in the shock wave region will be about 0.5 to 1 mag/200 pc, which will cause a great deal of absorption of starlight propagating tangentially through the shock lane. The strong absorption of starlight will be observed as locally-enhanced obscurations in the Milky Way. This is confirmed quantitatively on the basis of some model calculations as follows.

(i) Model distribution of diffuse starlight in the Milky Way with shock lanes along the spiral arms.

We calculate distributions of diffuse starlight the the Milky Way, assuming realistic models for the distribution of stars and absorbing matter, and the galactic

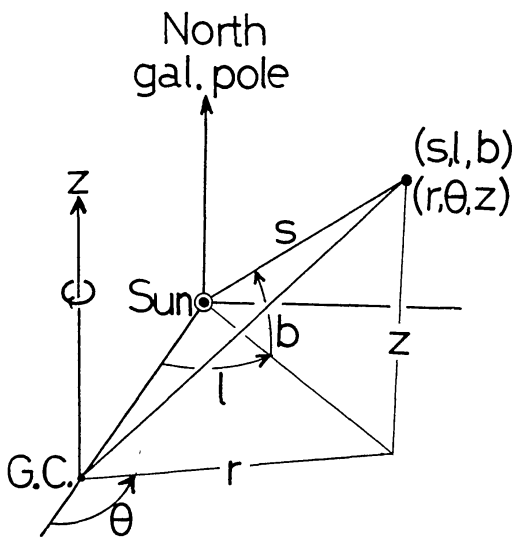

Fig. 4. Coordinate system used in the analysis. (s, l, b) are spherical coordinates with the origin at the sun. (r, θ, z) are cylindrical coordinates with the origin at the galactic center and with the axis parallel to the rotational axis of the Galaxy.

shock lanes along the spiral arms. The extinction coefficient of starlight determined in the solar vicinity will be made use of extensively in the calculations. Cylindrical coordinates system (r, θ, z) is used (figure 4), with the origin at the galactic center and with the z-axis parallel to the rotation axis of the Galaxy. Symbols l, b, and s designate the galactic longitude, latitude, and distance measured from the observer at the sun, respectively. The observer is assumed to be located on the galactic plane at a distance, R_0, from the galactic center.

Let ρ and ρ_a be the spatial densities of stars and absorbing matter, respectively, then the observed brightness is given by

$$I=\frac{1}{4\pi}\int_0^\infty [\varepsilon_s \rho \exp\{-\int_0^s a\rho_a ds\}]ds\ , \tag{1}$$

where I, ε_s, a, and s are the brightness of diffuse starlight, the light emissivity per unit mass of the stars, the absorption coefficient per unit column mass of interstellar gas and the distance in the line of sight, respectively. Here and hereafter, we ignore the contribution of scattered light to the total intensity.

The overall distribution of stars responsible for the galactic diffuse starlight is represented by

$$\rho(r, z)=\frac{Y_s(r)}{Z(r)}\exp\left\{-\frac{|z|}{Z(r)}\right\}\ , \tag{2}$$

where $Z(r)$ designates a local density scale-height in the z-direction, and $Y_s(r)$ is the surface density projected onto the galactic plane, for which we take one of TOOMRE'S (1966) models of disk galaxies, i.e.,

$$Y_s(r)=\frac{\sigma_s}{2}\left\{1+2\left(\frac{r}{r_{\max}}\right)^2\right\}^{-3/2}\ . \tag{3}$$

Here σ_s designates the surface density at the galactic center, and the rotation curve of the Galaxy attains its maximum at $r=r_{\max}$. We assume a similar form for the overall distribution of the interstellar gas,

$$\rho_{g1}(r, z)=\delta_1\frac{Y_s(r)}{\{\alpha_1 Z(r)\}}\exp\left[\frac{-|z|}{\{\alpha_1 Z(r)\}}\right], \tag{4}$$

where $\alpha_1 Z(r)$ is the vertical scale-height of the gas layer. Since the total amount of the mass of interstellar gas in the Galaxy is 1 to 3 percent of the total mass, we may take $\delta_1=0.01$ to 0.03.

TOSA (1973) has worked out the structure of the spiral shock wave by taking

into account of the vertical spread of the gas. He has shown that the effective z-thickness of the shock wave region is increased up to 1.2 to 1.5 times $\alpha_1 Z(r)$, and that the gas density just behind the shock front is 5 to 10 times that before it, depending on the magnitudes of the spiral potential and the magnetic field strength (see also FUJIMOTO 1966; ROBERTS 1969; ROBERTS and YUAN 1970). From this and for the convenience of numerical computation we assume the following form for the distribution of the gas density in the shock lane along the bisymmetrical logarithmic spiral,

$$\rho_{g2}=\delta_2 \frac{Y_s(r)}{\{\alpha_2 Z(r)\}} \exp\left[-\frac{|z|}{\{\alpha_2 Z(r)\}}\right] \sum_{\substack{i=0,1,2\cdots \\ j=1,2}} \xi_{ij} \exp\left\{-\frac{(r-R_{ij})}{\Delta}\right\}, \qquad (5)$$

with

$$\xi_{ij}\begin{cases} =1 & \text{for } r\geq R_{ij}\,, \\ =0 & \text{for } r<R_{ij}\,, \end{cases}$$

where $\alpha_2 Z(r)$ represents the vertical scale-height of the gas in the shock wave region.

The spiral is given by

$$R_{ij}=0.22R_0' \exp\left[0.12\{\theta+(j+2i)\pi\}\right], \quad (0\leq\theta<2\pi,\ i=0,1,2,\cdots), \qquad (6)$$

which is taken as to coincide with a spiral determined by MILLS (1959) when $R_0'=10$ kpc. Here $j=1$ and 2 correspond to the respective arms of the bisymmetric spirals and R_{ij}'s are the loci of the galactic shock front (figure 5).

The exponential factor in equation (5), $\exp\{-(r-R_{ij})/\Delta\}$, is used to approximate a sharp-edged distribution of the gas density in the shock wave region along the spiral arm (figure 6). The effective horizontal thickness of the shock wave is represented by Δ, which is 100 to 200 pc, and R_0' is the galacto-centric distance of the shock front nearest to the sun. Finally, the density scale-height in equations (2), (3), and (4) is assumed to vary as follows:

$$Z(r)=Z_c \exp\left\{-\left(\frac{r}{r_0}\right)^2\right\}, \qquad (7)$$

where Z_c is a density scale-height at the galactic center and r_0 is a constant.

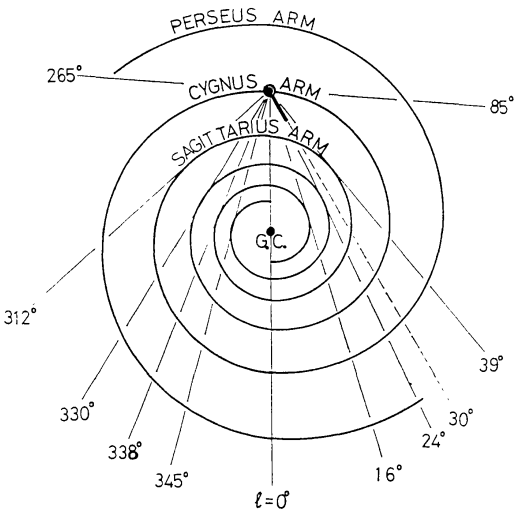

Fig. 5. Model spiral given by equation (6) (after MILLS [1959]). Position of the anti-Orion bridge assumed is shown by a thick line extending to $l=30°$ from the sun.

On the basis of these models, we carry out numerical integration of equation (1). The results are given in the form of contour diagrams of the brightness in the (l, b)-plane (figures 7a and 7b). The parameters used are

$R_0=10$ kpc,
$R_0'=9.7$ to 10 kpc,

$r_{max}=6.5$ kpc,
$r_0=10$ kpc,
$Z(R_0)=300$ pc (OORT 1959; HILL 1960),
$\alpha_1=0.33$ ($\alpha_1 Z(R_0)=100$ pc; ROUGOOR 1964),
$\alpha_2=0.4$ to 0.5 ($\alpha_2/\alpha_1=1.2$ to 1.5),
$\delta_2/\delta_1=6$,
$\Delta=100$ to 200 pc,

and the extinction coefficient, κ, is taken to be proportional to the gas density and is assumed to be 0.5 to 1 mag kpc^{-1} in the normal region in the solar neighborhood. The calculated results for the two cases of $\alpha_2/\alpha_1=1.5$ and 1.2 give qualitatively the same aspects for the starlight brightness.

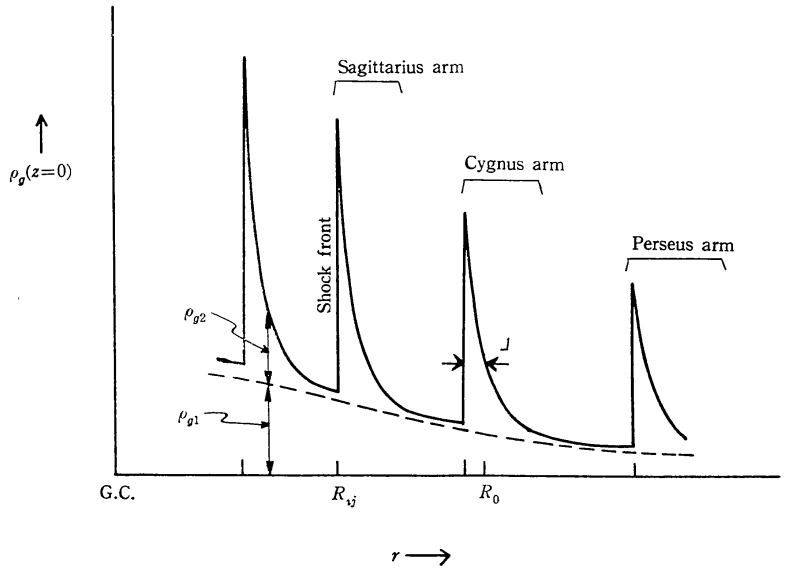

Fig. 6. Schematic illustrations of the distribution of the interstellar gas density versus the galacto-centric distance. ρ_{g2} is supposed to decrease exponentially with a scale-length, Δ, just behind the front of the galactic shock wave.

In the calculation of figure 7b, we have introduced the existence of the shock lane along a minor arm linking the Cygnus arm and the Sagittarius arm (the anti-Orion bridge). The bridge is assumed to be 2 kpc long, directed to $l=30°$ from a point 50 pc distant from the sun in the direction of $l=300°$, and situated slightly north of the galactic plane. Other parameters for this shock lane remain the same as before.

(ii) Dark lane along the galactic equator.

In the optical isophotes obtained by the model calculation, a dark lane is clearly reproduced along the galactic equator, except for the anticenter regions where the dark lane is not obvious. The feature is sufficiently compatible with the observed distribution of diffuse starlight as seen in figure 1: the dark lane at $b=0°$ is clearly observed in the direction near the galactic center but not in the anticenter regions.

The comparison between the calculated and observed diffuse starlight lead us to adopt the case of $\kappa=0.5$ mag kpc^{-1} rather than the case of $\kappa=1$ mag kpc^{-1}.

Therefore the interstellar extinction coefficient in the visual range will be close to 0.5 mag kpc^{-1} in the normal regions near the sun.

(iii) Locally enhanced obscurations of starlight; the Dark Regions.

We will discuss in more detail the comparison of the calculated and observed distributions of diffuse starlight.

(*a*) *Dark Region* (*92+07*): The direction tangential to the Cygnus arm coincides with the direction of this dark region. This is reproduced in the model isophotes as a deep dip of contour lines at $l=90°$ for the case of $R_0'=10$ kpc. If we take $R_0'=9.7$ kpc, the corresponding dark region appears at $l\approx 70°$.

(*b*) *Dark Region* (*265+03*): This model dark region is found at $l\approx 265°$ for $R_0'=10$ kpc and at $l\approx 275°$ for $R_0'=9.7$ kpc. This is located in the opposite direction to Dark Region (92+07) and is attributed to the Cygnus arm.

(*c*) *Dark Region* (25+05): This dark region is well reproduced as a large and deep dip of contour lines at $l\approx 30°$ in figure 7b in which a shock lane associated with the anti-Orion bridge is superimposed on the two logarithmic spirals.

(*d*) *Dark Region* (*135+00*): This is located in the direction of the region in the Perseus arm, at which an enhanced λ21-cm line emission of neutral hydrogen is observed. The present model, however, does not take into account of the local density fluctuations in the spiral arm, and hence the model calculation cannot reproduce this dark region. The situation is the same for Dark Region (180—05).

(*e*) *Dark Regions* (*55+05*), (*320+05*) *and other small ones* (*00+05*), (*13+00*), (*340+05*), (*340—05*): Dark Regions (55+05) and (320+05) are observed in the tangential directions of the Sagittarius arm. The present model gives only very slight dips of the contour lines in these directions. Other small dark regions are not reproduced. However, if the sun is located inside a shock lane, which is not unrealistic, the extinction coefficient of 0.5 mag kpc^{-1} is valid in the solar vicinity alone, and the extinction in the normal region may be $\sim$0.1 mag kpc^{-1} or less. If this smaller coefficient is correct, the small obscured regions can be sufficiently reproduced by the model calculation. Then they are understood as due to the tangential viewing of the distant spiral arms.

An alternative possibility is that these small dark regions are caused by local irregular distributions of obscuring matter in the solar vicinity. As is well known, many "fins" of dark matter at large angles to the luminous spiral arms are found in the photographs of extragalactic spirals. If such fins exist in the solar vicinity of the Galaxy, these small dark regions would be understood as the results of a tangential view of them. In this case, their spatial coincidence with the spiral arms is considered to be due only to chance.

In the present calculation, however, we cannot decide which is more plausible to explain the small dark regions near the galactic center including (55+05) and (320+05), i.e., the spiral shock lane of distant arm or the irregular distribution of absorbing matter, such as fins, in the solar vicinity.

4. *Interpretation of the Radio Spurs in Connection with the Galactic Shock Lane*

In this section, the radio continuum spur is interpreted as a nonthermal halo composed of magnetic fields and cosmic ray electrons situated above the galactic shock wave region. The inflation of the magnetic field and the diffusion of cosmic

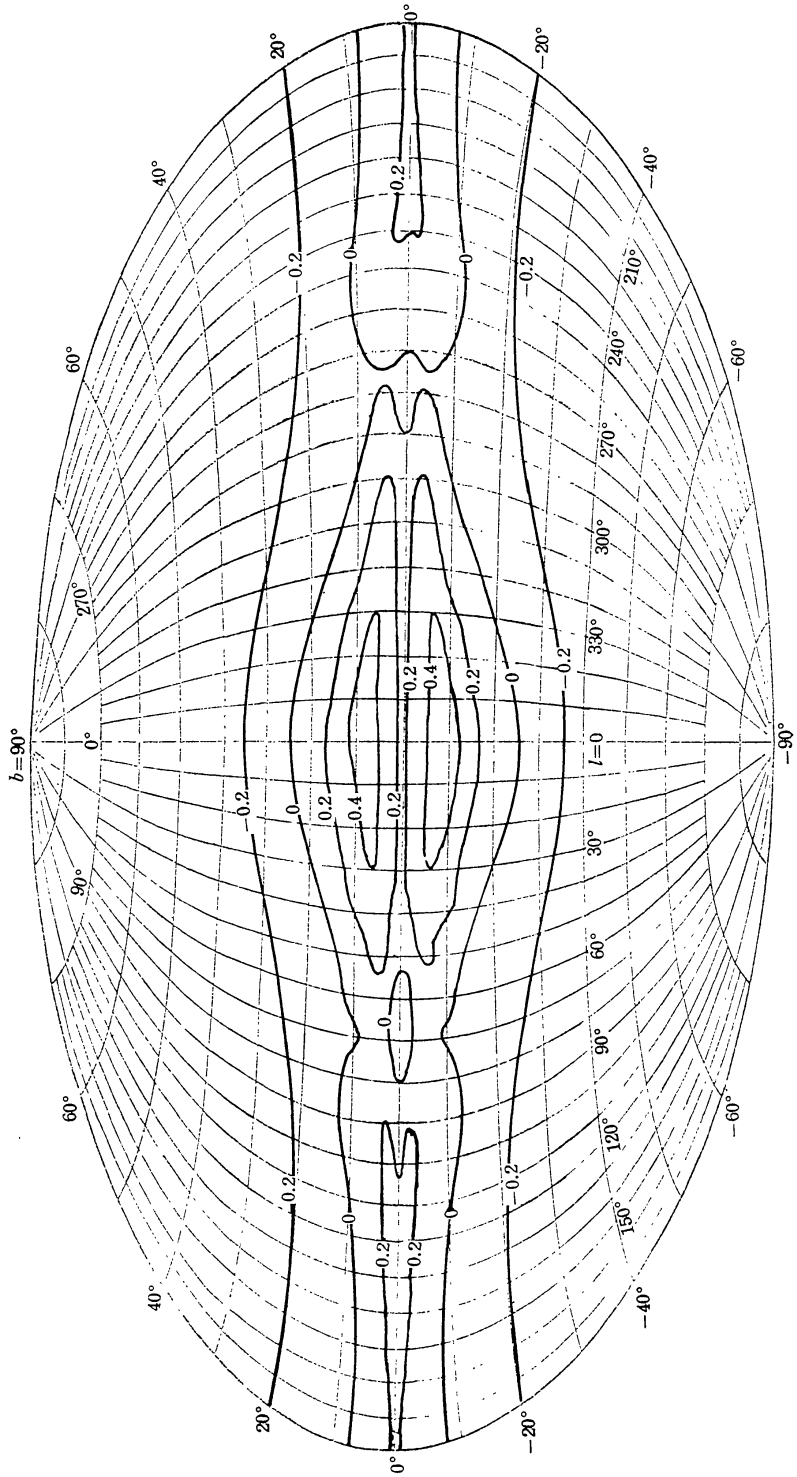

Fig. 7a. Contour diagram of calculated brightness distribution of the diffuse starlight in the (l, b)-plane for the case of $R_0'=9.7$ kpc, $\kappa=0.5$ mag kpc^{-1} and $\alpha_2/\alpha_1=1.5$. Indicated numerals on the contour lines give the logarithms of the brightness in an arbitrary unit, i.e., log I+arbitrary constant. Dark regions in tangential directions of the model shock lane along the Cygnus arm, as well as the dark lane along the galactic equator are seen.

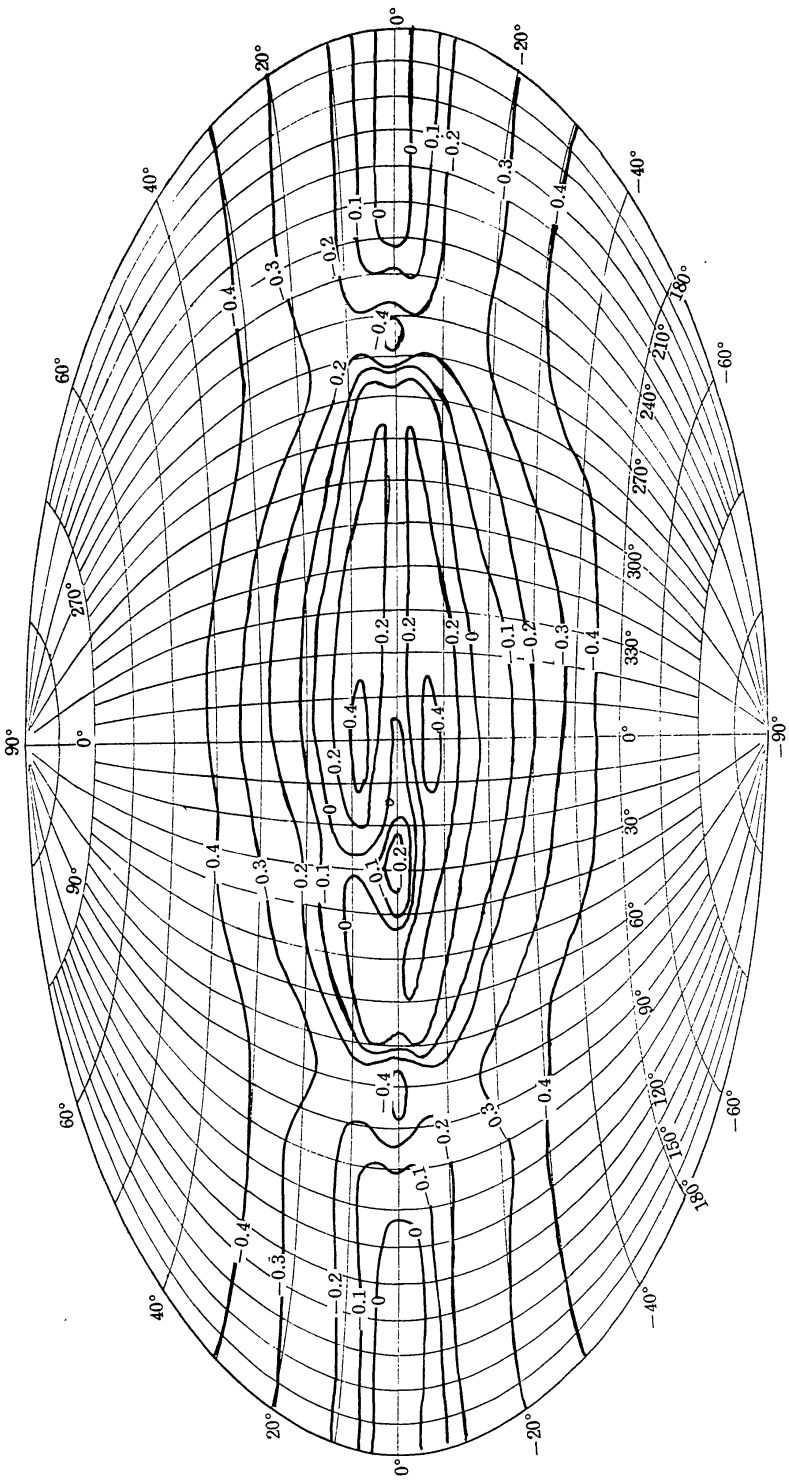

Fig. 7b. Same as figure 7a, for $R_0' = 10$ kpc and with the anti-Orion bridge superimposed. The great Dark Region (25+05) is reproduced by this model at $l \approx 30°$ as a deep dip of contours.

ray electrons out of the spiral arm into the galactic halo will be discussed in order to explain the origin of the nonthermal radio spur.

Interstellar gas in galactic rotation is suddenly compressed at the shock lane, and the density of interstellar nonthermal electrons is increased. The compression of the conducting gas will also amplify the magnetic field strength. Nonthermal radio emission from the shock lane will be, therefore, strongly enhanced compared with the normal region. Recently, MATHEWSON, VAN DER KRUIT, and BROUW (1972) have shown by observation with a high angular resolution at λ21 cm continuum that the radio emission is indeed strong along the dark lanes of the face-on galaxy M51. This observational fact supports the validity of FUJIMOTO's (1966) prediction for the galactic shock wave along the spiral arm.

In order to interpret the radio spurs in the Galaxy as a result of the strong compression of the interstellar gas with the cosmic ray electrons and magnetic fields at the shock lane, we calculate the brightness distribution of the nonthermal radiation from the model spiral arm accompanying the shock lane.

(i) Radio brightness distribution of the Galaxy.

Since the absorption of nonthermal radiation from spurs is negligible in the Galaxy, the brightness temperature, T, at a given wavelength is obtained by

$$T=K\int_0^\infty \varepsilon\, ds\,, \tag{8}$$

where K is a constant and ε is the volume emissivity. The integration is carried out along the line of sight.

The volume emissivity of synchrotron radiation is given by

$$\varepsilon=\frac{2e^4}{3m^2c^3}H_\perp{}^2\left(\frac{E}{mc^2}\right)^2 N(E) \tag{9}$$

at a frequency

$$\nu=\frac{1}{4\pi}\frac{eH_\perp}{mc}\left(\frac{E}{mc^2}\right)^2, \tag{10}$$

where E and $H_\perp$ are the energy of an electron responsible for the synchrotron radiation and the component of the magnetic field perpendicular to the line of sight, respectively. Other symbols have their usual meaning. The number density of the relativistic electrons is assumed to be

$$N(E)dE\propto E^{-\gamma}dE\,. \tag{11}$$

Relativistic electrons are trapped in the interstellar magnetic field and the field lines are frozen in the interstellar gas. The volume emissivity will change from ε to ε', corresponding to a change in the density of the gas from ρ_g to ρ_g',

$$\frac{\varepsilon'}{\varepsilon}=\frac{\rho_g'}{\rho_g}\left(\frac{E'}{E}\right)_{\rm ad}^{\gamma}\left(\frac{H_\perp'}{H_\perp}\right)^{(1+\gamma)/2}, \tag{12}$$

where $(E'/E)_{\rm ad}$ is the ratio of the energy of the relativistic electrons before and after the change in the gas density due to adiabatic compression. The Betatron and Fermi accelerations due to the temporal increase of the magnetic field strength in the shock region are not taken into account. The above quantities are then

written as follows:

$$\frac{H_{\perp}'}{H_{\perp}}=\left(\frac{\rho_g'}{\rho_g}\right)^{2/3}, \tag{13}$$

and

$$\left(\frac{E'}{E}\right)_{\mathrm{ad}}=\left(\frac{\rho_g'}{\rho_g}\right)^{\Gamma-1}, \tag{14}$$

where Γ represents the adiabatic exponent of the relativistic gas and $\Gamma=4/3$ is taken. Here random configurations of magnetic fields have been assumed. Equation (12) yields

$$\frac{\varepsilon'}{\varepsilon}=\left(\frac{\rho_g'}{\rho_g}\right)^{(2/3)\gamma+(4/3)}. \tag{15}$$

If magnetic lines of force are parallel to the spiral arm, expression (15) will be modified to

$$\frac{\varepsilon'}{\varepsilon}=\left(\frac{\rho_g'}{\rho_g}\right)^{(3/2)+\gamma\{\Gamma'-(1/2)\}}(\sin\varphi)^{(\gamma+1)/2}, \tag{16}$$

where φ is the angle between the direction of the magnetic field and the line of sight, and Γ' is the adiabatic exponent of the relativistic gas for one-dimensional compression perpendicular to the magnetic field. (Isotropic motions of nonthermal electrons have been assumed throughout the above estimates.)

Hereafter we will assume that the direction of the magnetic field is randomly distributed and equation (15) holds entirely in the Galaxy. Then the distribution of the brightness temperature of nonthermal radio emission is obtained by

$$T=\mathrm{const.}\int_0^{\infty}\rho_g^{(2/3)\gamma+(4/3)}ds. \tag{17}$$

In figures 8a to 8c are shown the brightness distributions in the (l, b)-plane calculated from equations (4), (5), (6), and (17). Parameters used are the same as in section 3, except for the vertical scale-height of the radio-emitting regions along the shock lane. Here $\gamma=2.4$ (OKUDA and TANAKA 1968) has been taken. In these figures the relative brightness is given.

(ii) Model radio isophotes.

We have calculated the brightness for some cases with different scale-heights for radio-emitting regions, $\alpha_2'Z(r)$, where α_2' should be replaced with α_2 in equation (5). If α_2' is taken equal to the values used in section 3, that is, if the scale-height of the radio-emitting region along the shock lane is equal to that of the interstellar gas, only slight spur-like features appear in the model isophotes (figure 8a). On the other hand, when we take $\alpha_2'=2$ to 3, the model radio spurs become very similar to the observed ones (figure 8b). In this case, the scale-height of the radio emitting regions associated with the shock lane is 0.6 to 1 kpc in the solar vicinity.

From their observation of neutral hydrogen gas at intermediate latitudes up to $b\approx 20°$, KEPNER (1970) and OORT (1970) have found that a "bank" of HI-gas clould is situated directly above the spiral arm in the galactic plane. This observation is suggestive of the existence of gaseous halos along the spiral arm.

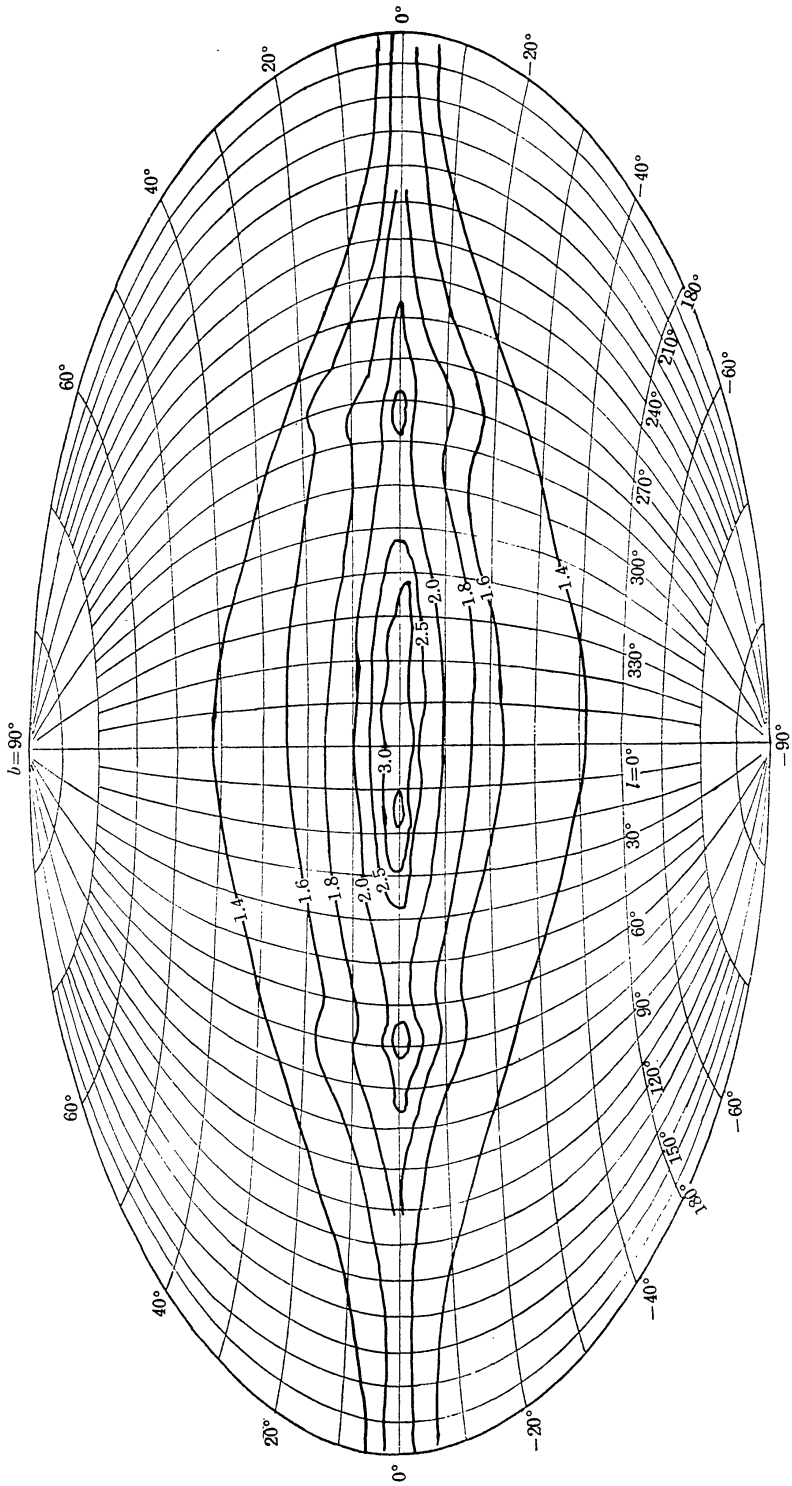

Fig. 8a. Contour diagram of calculated brightness of the nonthermal radio emission in the (l, b)-plane, for the case of $R_0'=9.7$ kpc and $\alpha_2'=0.5$. Indicated numerals on the contour lines are logarithms of the brightness temperature in an arbitrary unit, i.e., $\log T+$arbitrary constant. Only a slight spur-like feature appears in this case.

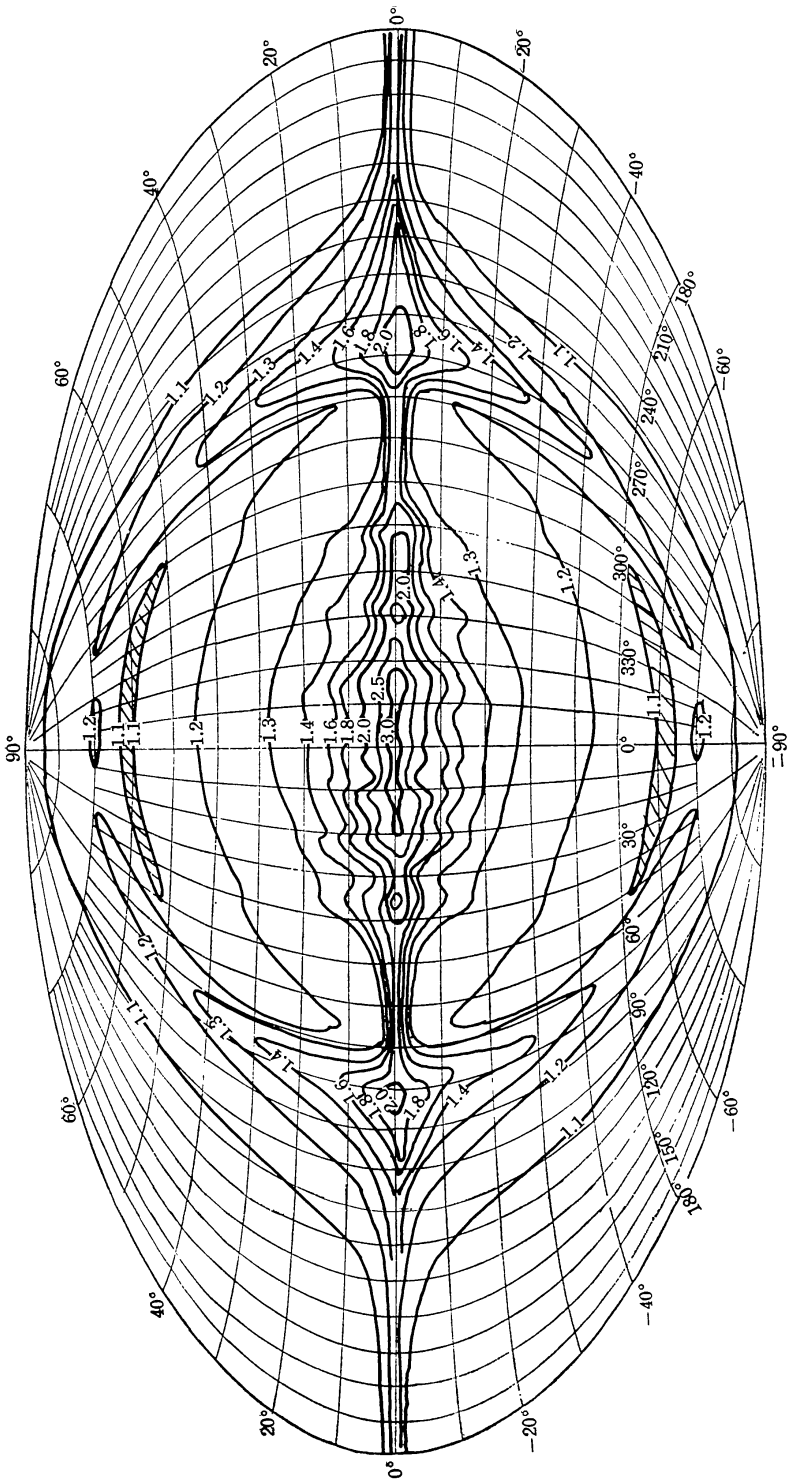

Fig. 8b. Same as figure 8a, for $R_0'=10$ kpc and $\alpha_2'=2$. Radio spurs being located in the tangential directions of the model shock lane are found.

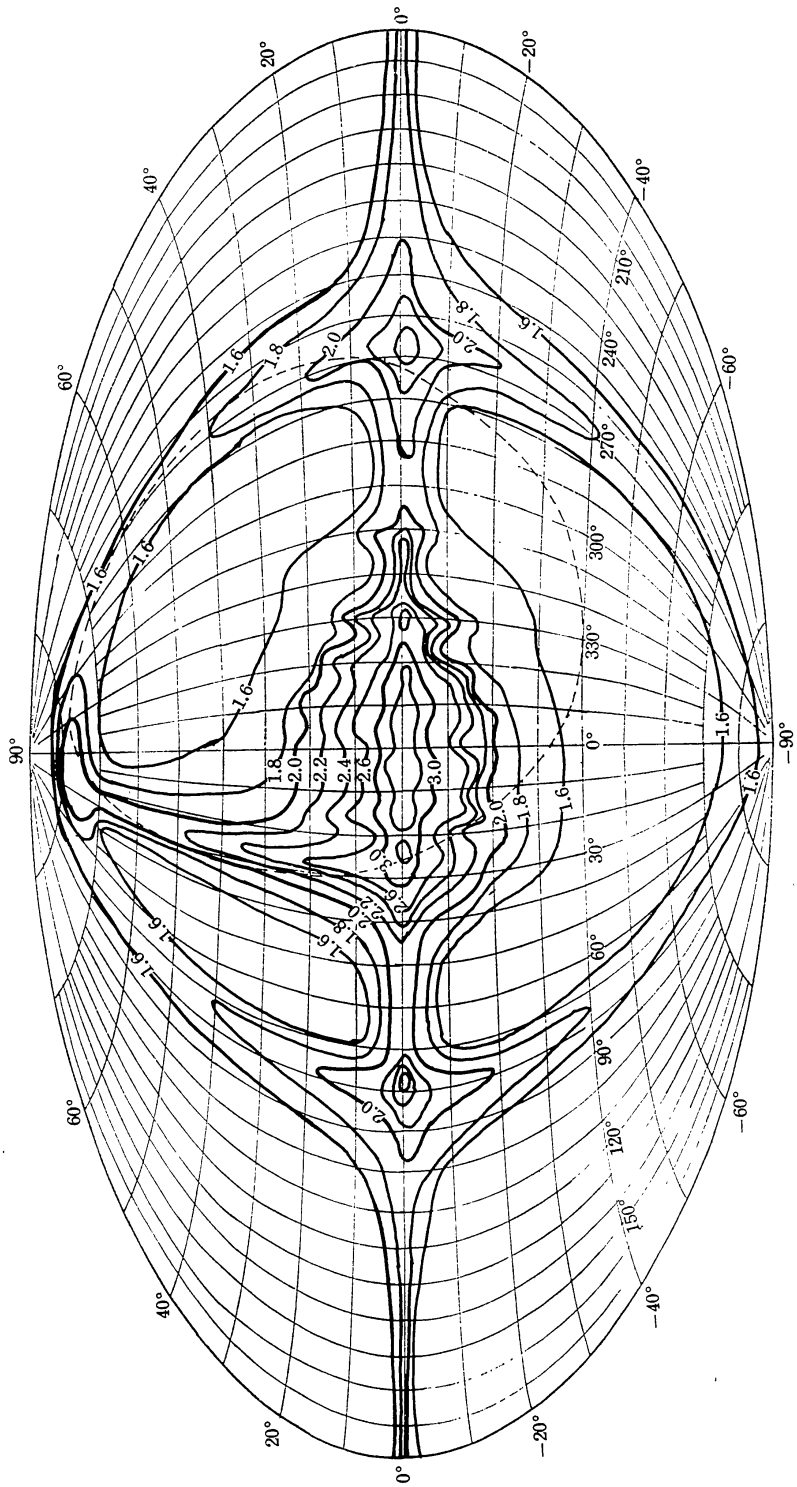

Fig. 8c. Same as figure 8b, with the anti-Orion bridge superimposed. The North Polar Spur is reproduced as a large hump of contours at $l \approx 30°$. The dashed curve is a small circle determined by BERKHUIJSEN et al. (1971) to fit the observed North Polar Spur (Loop I).

The vertical scale-height of this halo may be 1 to 2 kpc. This value of vertical spread is in agreement with that for the nonthermal halo chosen in the present calculations. On the other hand, since small radio spurs observed near the galactic center, for example, at $(l, b)\approx(10°, 20)$, $(340°, 20°)$, and $(10°, 20°)$ (figures 2a and 3) which extend up to $b\approx20°$, are considered to be associated with the inner arms of the Galaxy, then the scale-height of corresponding nonthermal halos becomes again $\sim$2 kpc. It is therefore plausible that the radio halos are situated above the spiral shock lane (nonthermal radio bank) with a vertical scale-height of 1 kpc, and with a horizontal thickness of about 200 pc.

In addition to the large model spurs at $l\approx90°$ and 270°, there are many small spurs with wavy iso-brightness contours in the galactic longitudes 320° to 40°. It is to be noted that small, similar spurs are observed in the same longitude range (figure 2a). It is reasonable to accept that the observed small spurs around the direction of the galactic center are due to the tangential viewing of the radio halos associated with the inner arms of the Galaxy. The observed radio spurs in the anticenter directions such as at $l\approx150°$ or at 180° would be due to the locally-enhanced condensations of gas in the Perseus arm. However, since the local irregularity of gas in the arm has not been taken into account, we cannot treat these spurs in the scheme of the present model.

(iii) North Polar Spur.

HANBURY BROWN, DAVIES, and HAZARD (1960) have suggested that the North Polar Spur is associated with a minor arm linking the Cygnus arm and Sagittarius arm, with which we have identified the anti-Orion bridge of neutral hydrogen gas in section 3 in order to reproduce the great dark region at (25+05) in the model isophotes of diffuse starlight. HANBURY BROWN et al. (1960) have considered this spur to be due to radio emitting regions whose configuration is cylindrical and which is located parallel to and above the galactic plane. According to our hypothesis, however, it is regarded as a nonthermal halo produced by a strong shock wave at the anti-Orion bridge of interstellar gas.

We have calculated the radio brightness distribution assuming the same shock lane along the anti-Orion bridge as assumed in section 3, which extends to the direction $l=30°$ and links the Cygnus and Sagittarius arm. The parameters are taken to be the same as those in the above section, except for the value of $\alpha_2'=3$.

Figure 8c shows the calculated result. The model North Polar Spur appears at $l\approx30°$. It has a sharper edge at the equatorially northern side of the ridge than at the southern side. This is due to the assumption that the sun is not in the shock front in the anti-Orion bridge. This result is qualitatively in agreement with the observed sharper northern edge of the North Polar Spur (BLYTHE 1957; HASLAM, LARGE, and QUIGLEY 1964).

The presently calculated North Polar Spur composes a loop-shaped ridge, being linked with the spur extending from $l\approx270°$ and $b\approx0°$. The dotted curve in figure 8c is the small circle determined by BERKHUIJSEN et al. (1971) (see also QUIGLEY and HASLAM 1965) to fit the North Polar Spur (Loop I), which also well fits the calculated spurs. It should be noticed that the shell-structured source, as is generally speculated in the supernova remnant hypothesis of spurs (see section 5), is not always necessary to interpret a loop-shaped ridge in the contour map.

(iv) Origin of the radio spurs.

The PARKER (1966, 1969)-type instability of inflation of the interstellar mag-

netic fields with cosmic ray gas out of the gaseous disk will be effective for the formation of the nonthermal halos. The inflation will be promoted by the strong compressions of gas and magnetic fields in the galactic shock region. It is reasonable to consider that the field strength and the high energy electron density in the halo along the shock lane will be greater, where the radio emission responsible for the radio spur will be correspondingly increased. If this is the case, the magnetic lines of force above the shock lane will be stretched into the halo perpendicular to the galactic plane; the field observed will be parallel to the ridge of a spur changing the sense of the direction with a small displacement of the line of sight. Figure 9 illustrates schematically the three dimensional structure of the spiral arm accompanying the shock lane and the radio halo along it.

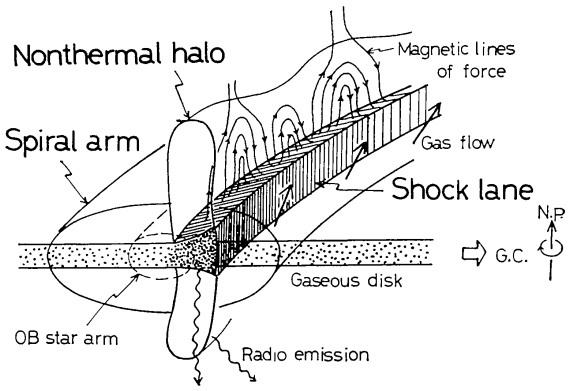

Fig. 9. Schematic illustration of the cross section of the spiral arm accompanying a shock lane and a radio halo (nonthermal radio bank) responsible for the radio spur.

Measurements of starlight polarizations (MATHEWSON 1968; MATHEWSON and FORD 1970), in fact, show that apparent directions of the magnetic field in some spurs are parallel to their ridges. On the other hand, GARDNER, WHITEOAK, and MORRIS (1967) have found that the values of rotation measure of the Faraday effect for extragalactic radio sources are large, while it reverses sense for directional displacement of a few degrees, in two narrow areas around $(l, b)\simeq(180°, -30°)$ and $(15°, 10°)$. The former region coincides with a large H I-spur and the latter with the region of an enhanced concentration of H I-gas, as can be seen from figure 2b. GARDNER et al. (1967) have suggested that this phenomenon can be explained by magnetic fields pulled out of the spiral arm by the gas flow. In such a model, the line-of-sight field can be large while its sense can reverse for small changes of direction. These two observational facts concerning galactic magnetic fields are in good agreement with our picture for the formation of radio spurs.

5. *On the Supernova Remnant Hypothesis of the Spurs and the North-South Asymmetry.*

(i) The supernova remnant hypothesis of spurs.

A supernova remnant hypothesis proposed by HANBURY BROWN, DAVIES, and HAZARD (1960) has been widely accepted as one of the most promising interpretations of the North Polar Spur. However, this hypothesis is not always satisfactory in view of the following observational facts.

First, if the three well-known spurs (North Polar Spur [Loop I], Loop III, and Cetus Arc [Loop II]) are due to supernova remnants with shell structures, then their distance from the sun will be at most 100 pc. Now, if all these loops were produced by independent supernova explosions, the probability that they are located so close to the sun at the same time by chance will be $\sim 3\times10^{-5}$, because the

probability that we find a supernova remnant within a distance of 100 pc from us is 1/30 (HANBURY BROWN et al. 1960). SHKLOVSKY (1968) has estimated the probability of finding the North Polar Spur and Cetus Arc as supernova remnants 30 pc apart from the sun, giving a vanishingly small value, 10^{-5} to 10^{-6}. If we adopt 30 pc for the distance to the above three supernova remnants, the probability to find them in such a small volume by chance decreases to 10^{-9}. This small probability would make it extremely difficult to accept the supernova remnant hypothesis.

Next, if the radio spur is due to radio emission from a supernova remnant, the iso-brightness contours should be nearly circular and the brightness must be more or less uniform along the circular loop. However, if we approximate the North Polar Spur, Cetus Arc, and Loop III by circular loops, their brightness distributions are far less uniform along the loops. Indeed, the ridges of the spurs have their origins at the galactic equator and do not cross over it, without completing a loop (BINGHAM 1967; BERKHUIJSEN et al. 1971).

Finally, no obvious evidence for the existence of Hα emission filamentary structure, which is characteristic of supernova remnants like Cygnus Loop, is found in these spurs (DAVIES, HANBURY BROWN, and MEABURN 1963). In addition, as shown in section 2, neutral hydrogen gas and the dust lanes are connected with the spurs. Such situations cannot be interpreted by the supernova remnant hypothesis.

On the other hand, ODA and HASEGAWA (1962) have proposed a cigar-shaped configuration of cosmic ray clouds produced by a supernova explosion as an explanation of the North Polar Spur. They have argued that the cosmic ray gas in a regular magnetic field expands along the field lines and hence will be observed as a cigar-shaped bright belt of nonthermal radio emission.

According to this hypothesis, all the observed radio spurs should be parallel to the magnetic field of the Galaxy. Moreover, a spur should have two parallel ridges of contours along the major axis of the cigar-shaped cloud, because the magnetic fields are stronger at the surface of the expanding cloud. The former speculation will be excluded by the fact that all the observed spurs extend almost perpendicular to the galactic plane. The latter is also not compatible with the observed features of the spurs.

Hence, both the supernova hypotheses described above seem to encounter with many difficulties when the spurs, including many small ones, are investigated systematically.

(ii) Galactic north-south asymmetry of radio spurs.

Although our model reproduces well the representative features of observed dark regions and radio spurs such as Dark Region (25+05) and the North Polar Spur, detailed features such as a galactic north-south asymmetry in the observed distributions still remain open to question.

Neutral hydrogen gas is not distributed exactly on the galactic plane but at different heights of the order of 40 pc below and above the plane, and the gaseous disk is observed to be radially "corrugated" with a characteristic wavelength of $\sim$3 kpc (VARSAVSKY and QUIROGA 1970). If we take account of this observational fact, the theory of the galactic shock wave, including the vertical spread of the gas (TOSA 1973) leaves the possibility of presenting an asymmetric feature of the vertical extension of the shock lanes and will provide a theoretical basis for understanding the north-south asymmetry of the radio spurs. This problem is,

however, beyond the scope of the present paper.

In order to see what features appear when a north-south asymmetry of the vertical spread of the model shock lanes is taken into account, we have calculated the optical and radio brightness distributions for the following case; the galactic shock waves, as well as the radio halos, are located above the galactic plane in an arm of the bisymmetrical spirals and below in another arm. The calculated optical isophotes give similar features to figure 7a, except for the dark regions which appear only in the northern side of the galactic plane as deep dips of contour lines near the tangential directions of the Cygnus arm. The model radio spurs at $l \approx 90°$ and 270°, both belonging to the Cygnus arm, extend into the northern hemisphere alone. Those near the galactic center appear alternatively above and below the galactic equator as the longitude varies. These features are in better agreement with observation.

6. *Conclusions*

The galactic radio spurs and the neutral hydrogen spurs have been found to be spatially associated with the optically dark patches in the Milky Way. They also coincide with the tangential directions of the neutral hydrogen arms of the Galaxy and with Mills steps of meter-wavelength radio emission. These observational facts suggest that the radio spurs have physical connections with the spiral structure of the Galaxy.

The optically obscured regions in the Milky Way are interpreted as having resulted from the tangential viewing of the shock wave region along the spiral arm, where the absorbing matter is condensed by the same factor as the gas density. Model calculation of the distributions of diffuse starlight, assuming the galactic shock waves along the arms, reproduce well the observed distributions. An especially large dark region at $l=20°-30°$ and $b=0°-10°$ is understood as a result of viewing from the inside of the shock lane along the anti-Orion bridge which links the Cygnus arm and the Sagittarius arm in the solar vicinity.

The radio spurs are interpreted as being due to tangential views of the nonthermal halos distributed along and above the galactic shock wave regions. The radio halos along the shock lane responsible for the spur will be produced by inflation of the magnetic fields out of the galactic spiral arm in which the inflation is promoted by the shock wave. From model calculations of the radio brightness distributions, it is required that nonthermal halo should be distributed along the shock lane with a vertical scale-height of ~ 1 kpc in order to reproduce the spurs.

The supernova remnant hypothesis of spurs seems to be encumbered with many difficulties. The galactic north-south asymmetry of the spurs remains difficult to explain theoretically. However, the "corrugated" structure observed for the disk of neutral hydrogen gas in the Galaxy would provide a key to this problem. The three-dimensional analysis of the shock wave along the spiral arm, including the asymmetric motion of gas in the z-direction, could give a theoretical basis to this phenomenon.

The author wishes to express his hearty thanks to Professor M. Fujimoto for valuable discussions and for a critical reading of the manuscript. Numerical computations were carried out on a FACOM 230-60 at the Nagoya University. He is indebted to the Lund Observatory for providing him the composite panorama of

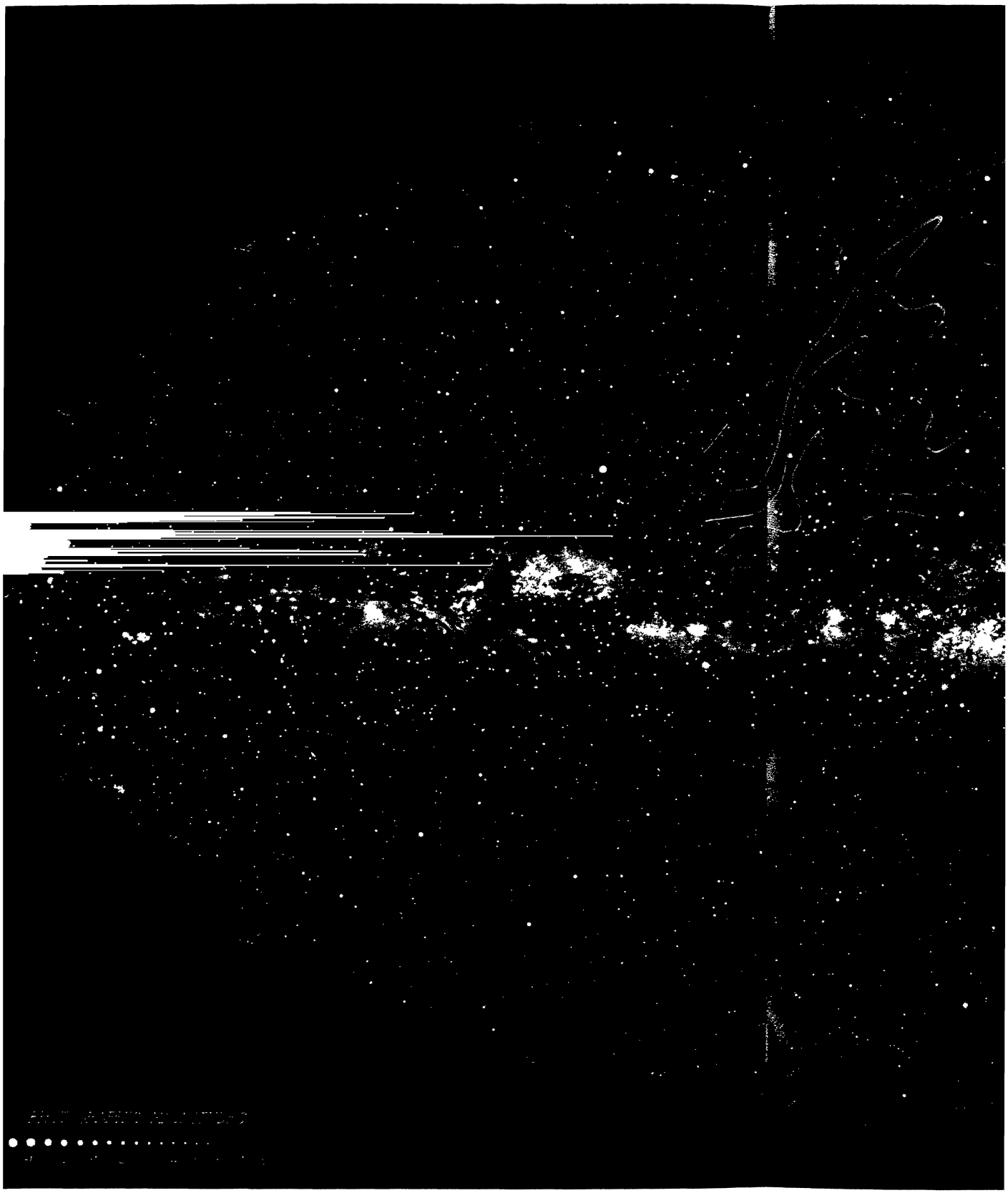

Fig. 1. Composite panorama of the Milky Way (Copyright © by the Lund Observatory; note that the indicated coordinate
It should be noticed that the North Polar Spur at radio continuum (indicated with contour lines) is associated with thi

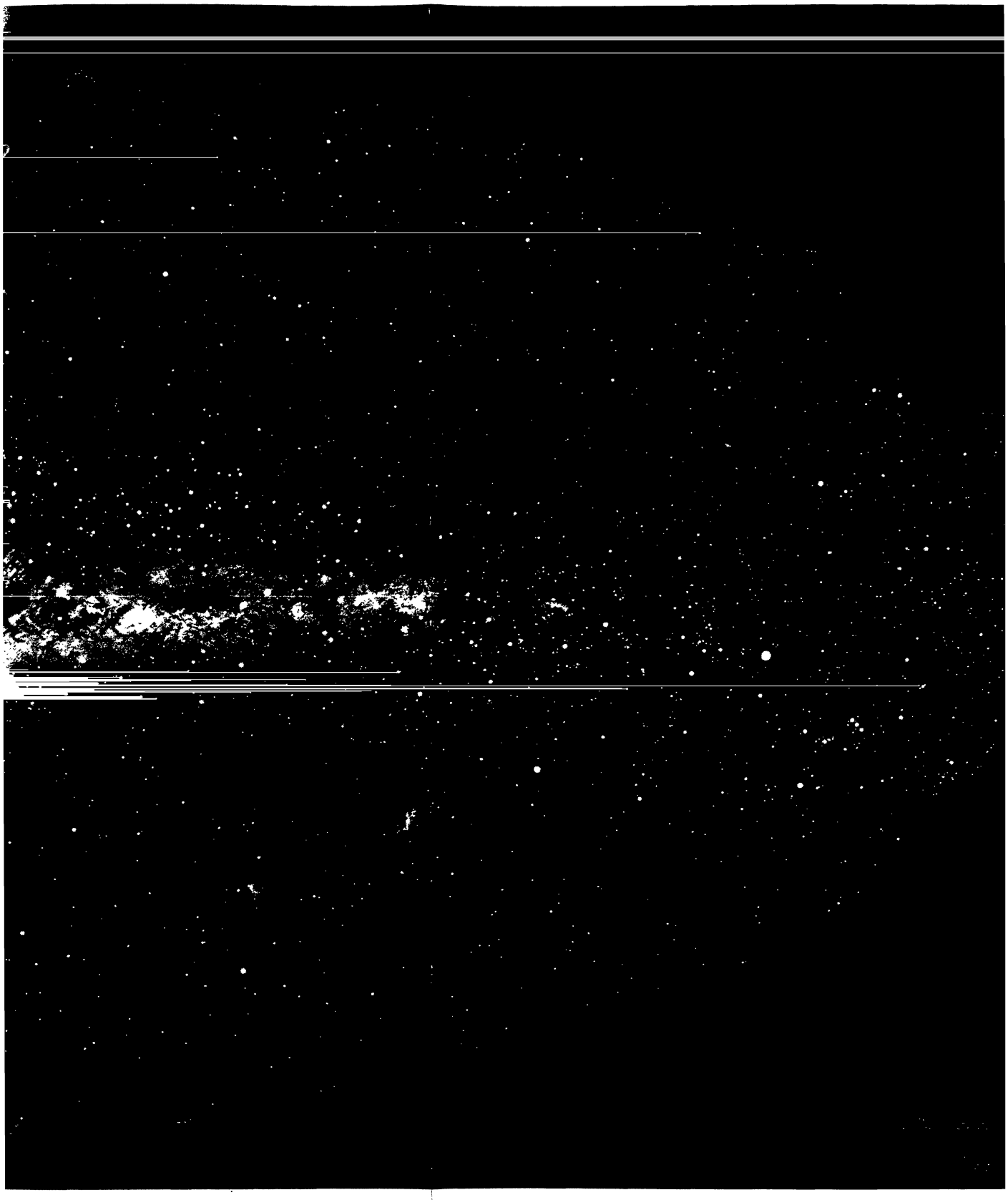

l^I and b^I and the center of this map is at $l^I=320°$ [$l=352°$]). A large dark region at $l=20°—30°$ and $b=0°—10°$ is remarkable.
ɛ area.

the Milky Way.

References

BERKHUIJSEN, E.M., HASLAM, C.G.T., and SALTER, C.J. 1970, *Nature*, **225**, 364.

BERKHUIJSEN, E.M., HASLAM, C.G.T., and SALTER, C.J. 1971, *Astron. Astrophys.*, **14**, 252.

BINGHAM, R.G., 1967, *Montly Notices Roy. Astron. Soc.*, **137**, 157.

BLYTHE, J.H. 1957, *Monthly Notices Roy. Astron. Soc.*, **117**, 652.

DAVIES, R., HANBURY BROWN, R., and MEABURN, J. 1963, *Observatory*, **83**, 179.

ELSÄSSER, H., and HAUG, U. 1960, *Z. Astrophys.*, **50**, 121.

FUJIMOTO, M. 1966, in *Non Stable Phenomena in Galaxies. IAU Symposium, No. 29*, ed. M. Arakeljan (Academy of Sciences of Armenia SSR), p. 453.

GARDNER, F.F., WHITEOAK, J.B., and MORRIS, D. 1967, *Nature*, **214**, 371.

HANBURY BROWN, R., DAVIES, R.D., and HAZARD, C. 1960, *Observatory*, **80**, 191.

HASLAM, C.G.T., LARGE, M.I., and QUIGLEY, M.J.S. 1964, *Monthly Notices Roy. Astron. Soc.*, **127**, 273.

HILL, E.R. 1960, *Bull. Astron. Inst. Neth.*, **15**, 1.

KEPNER, M. 1970, *Astron. Astrophys.*, **5**, 444.

KERR, F.J., and WESTERHOUT, G. 1965, in *Galactic Structure*, ed. A. Blaauw and M. Schmidt (University of Chicago Press, Chicago), p. 167.

MATHEWSON, D.S. 1968, *Astrophys. J. Letters*, **153**, L47.

MATHEWSON, D.S., and FORD, V.L. 1970, *Mem. Roy. Astron. Soc.*, **74**, 139.

MATHEWSON, D.S., KRUIT, P.C. VAN DER, and BROUW, W.N. 1972, *Astron. Astrophys.*, **17**, 468.

MCGEE, R. X., MURRAY, J.D., and MILTON, J.A. 1963, *Australian J. Phys.*, **16**, 136.

MILLS, B.Y. 1959, in *Paris Symposium on Radio Astronomy, IAU Symposium, No. 9*, ed. R.N. Bracewell (Stanford Univ. Press, Stanford, California) p. 431.

ODA, M., and HASAGAWA, H. 1962, *Physics Letters*, **1**, 239.

OKUDA, H., and TANAKA, Y. 1968, *Bull. Astron. Inst. Neth.*, **20**, 129.

OORT, J.H. 1959, *Bull. Astron. Inst. Neth.*, **15**, 45.

OORT, J.H. 1970, in *The Spiral Structure of Our Galaxy, IAU Symposium, No. 38*, ed. W. Becker and G. Contopoulos (D. Reidel Publ. Co., Dordrecht, Holland), p. 142.

PARKER, E.N. 1966, *Astrophys. J.*, **145**, 811.

PARKER, E.N. 1969, *Space Sci. Rev.*, **9.**, 651.

QUIGLEY, M.J.S., and HASLAM, C.G.T. 1965, *Nature*, **208**, 741.

ROBERTS, W.W. 1969, *Astrophys. J.*, **158**, 123.

ROBERTS, W.W., and YUAN, C. 1970, *Astrophys. J.*, **161**, 887.

ROUGOOR, G.W. 1964, *Bull. Astron. Inst. Neth.*, **17**. 381.

SEEGER, C.L., STUMPERS, F.L.H.M., and HURCK, N. VAN, 1966, *Philips Tech. Rev.*, **21**, 317.

SEEGER, C.L., WESTERHOUT, G., CONWAY, R.G., and HOEKEMA, T., 1965, *Bull. Astron. Inst. Neth.*, **18**, 11.

SHKLOVSKY, I.S. 1968, *Supernova* (John Willey and Sons Ltd., London), p. 377.

TAKAKUBO, K., and WOERDEN, H. VAN, 1966, *Bull. Astron. Inst. Neth.*, **18**, 488.

TOLBERT, C.R. 1971, *Astron. Astroprys. Suppl.*, **3**, 349.

TOOMRE, A. 1966, *Astrophys. J.*, **138**, 385.

TOSA, M. 1973, *Publ. Astron. Soc. Japan*, **25**, 191.

VARSAVSKY, C.M., and QUIROGA, R.J. 1970, in *The Spiral Structure of Our Galaxy, IAU Symposium, No. 38*, ed. W. Becker and G. Contopoulos (D. Reidel Publ. Co., Dordrecht, Holland), p. 147.